Matkovic et al., http://www.jcb.org/cgi/content/full/jcb.201301072/DC1

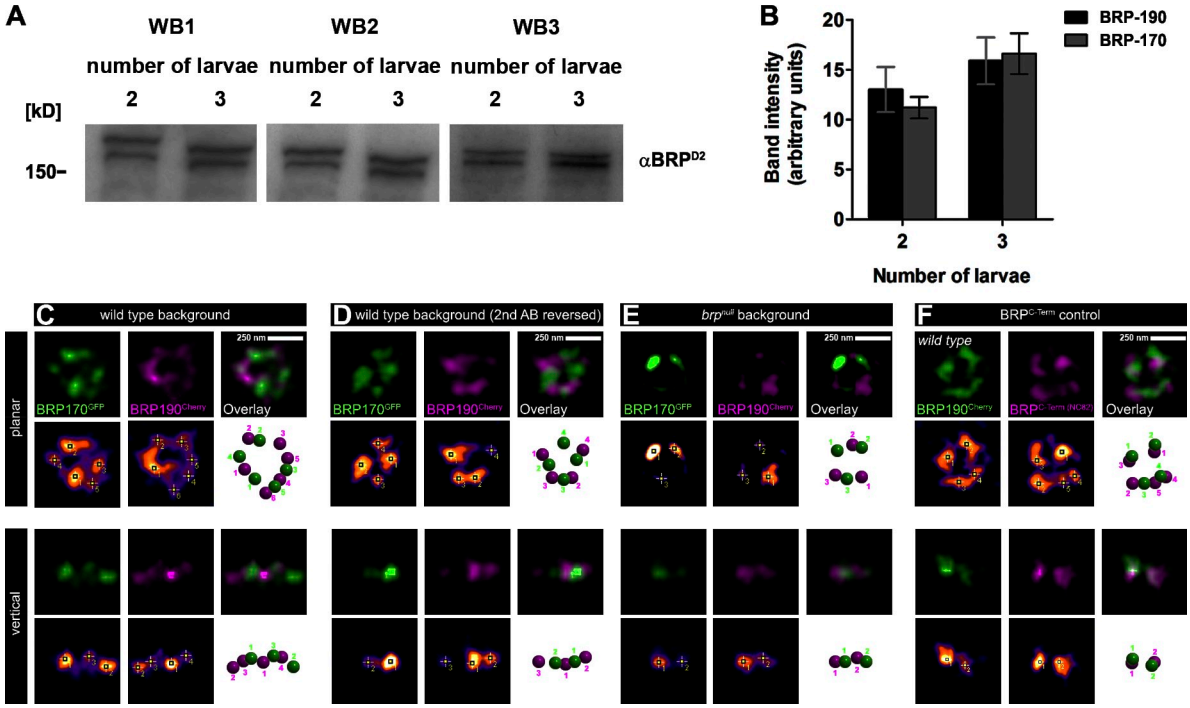

Figure S1. **BRP isoform larval protein levels and additional analysis of distribution.** (A) Western blots of *Drosophila* wild-type larval body walls for relative quantification of BRP isoform protein levels. Three independent experiments with two and three larvae loaded were conducted, and membranes were probed with anti-BRP^{D2}. The two bands of 190- and 170-kD apparent sizes represent the BRP-190 and BRP-170 isoforms, respectively. (B) Quantification of the Western blots shown in A by densitometric readout revealed equal abundance of BRP-190 and BRP-170 in wild-type larval body walls (two larvae: BRP-190, 13.0 ± 2.3; BRP-170, 11.2 ± 1.1; P = 0.7; *n* = 3; three larvae: BRP-190, 15.9 ± 2.4; BRP-170, 16.6 ± 2.0; P = 1.0; *n* = 3; Mann–Whitney *U* test). Data are expressed in arbitrary units of intensity. Error bars represent SEMs. (C–F) Planar- and vertical-oriented AZs imaged with two-color STED resolution. Bottom images show the same channels displayed with the fire lookup table and with the maxima highlighted by the find maxima function of ImageJ (default settings). The respective third images show manual reconstructions of the punctae based on merges of the respective former two images. (C) BRP-170^{GFP} stained with anti–mouse GFP and anti–mouse Atto647N, BRP-190^{Cherry} stained with anti–rabbit dsRed and anti–rabbit Atto594 in wild-type background. (D) BRP-170^{GFP} stained with anti–mouse GFP and anti–mouse Atto594, and BRP-190^{Cherry} stained with anti–rabbit dsRed and anti–rabbit Atto647N in a wild-type background. (E) BRP-170^{GFP} stained with anti–mouse GFP and anti–mouse Atto594 and BRP-190^{Cherry} stained with anti–rabbit dsRed and anti–rabbit Atto647N in *brp^{null}* background. (F) BRP-190^{Cherry} stained with anti–rabbit dsRed and anti–rabbit Atto647N and BRP$^{C\text{-}Term\ (NC82)}$ stained with anti–mouse Atto594 in a wild-type background.

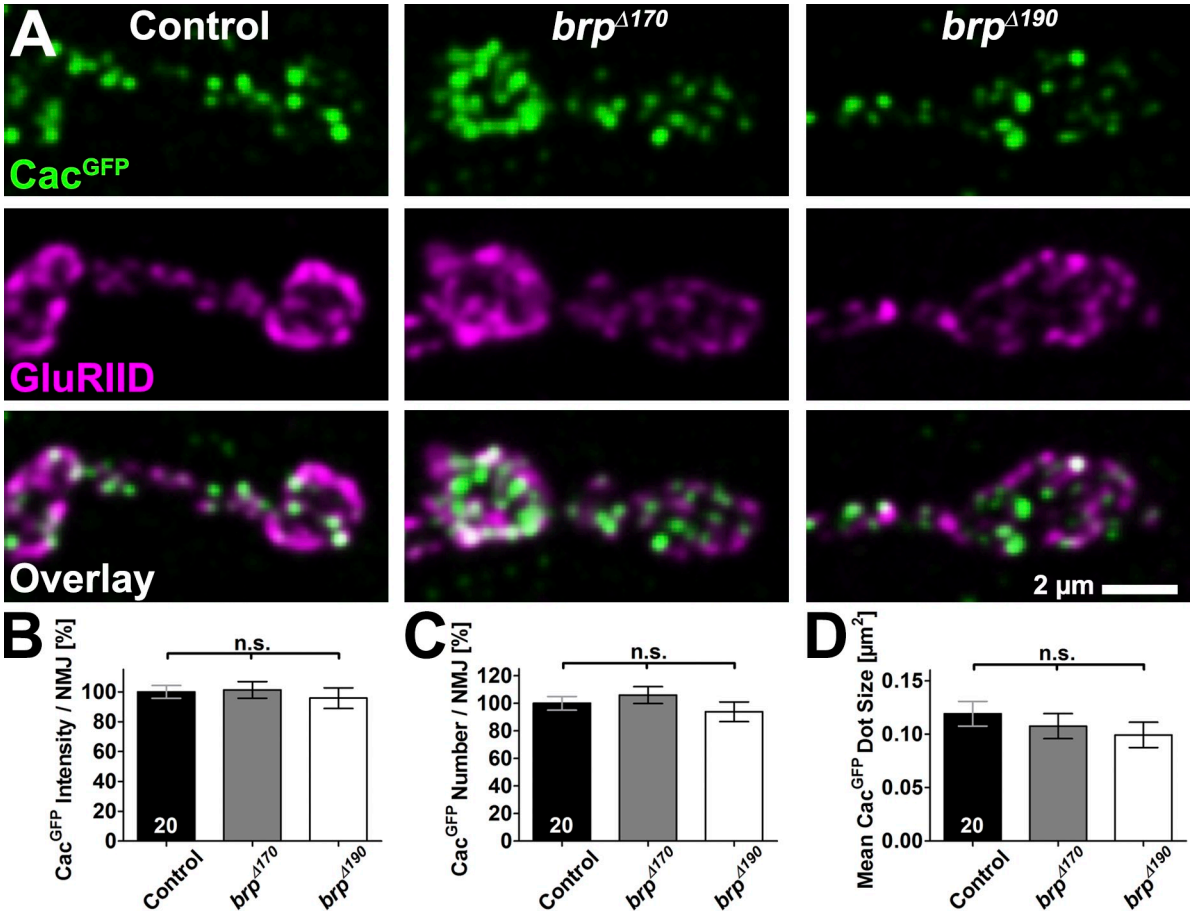

Figure S2. **Ca^{2+} channel clustering is not affected in BRP isoform mutants.** (A) Two boutons of NMJs on muscle 4 from third instar larvae with the indicated genotypes, labeled with the indicated ABs. (B) Quantification of Cac^{GFP} intensity measured over the whole NMJ (HRP mask). Control, 100.0 ± 4.3; $brp^{\Delta 170}$, 101.3 ± 5.6, P = 0.9461 versus control; $brp^{\Delta 190}$, 95.8 ± 6.9, P = 0.1479 versus control and P = 0.1896 versus $brp^{\Delta 170}$; *n* = 20 NMJs in seven larvae/genotype. (C) Quantification of the number of Cac^{GFP} dots measured over the whole NMJ (HRP mask). Control, 100.0 ± 4.9; $brp^{\Delta 170}$, 106.0 ± 6.2, P = 0.2559 versus control; $brp^{\Delta 190}$: 93.9 ± 7.1, P = 0.3104 versus control and P = 0.0658 versus $brp^{\Delta 170}$; *n* = 20 NMJs in seven larvae/genotype. (D) Quantification of Cac^{GFP} dot size per AZ. Control, 0.12 ± 0.01; $brp^{\Delta 170}$, 0.11 ± 0.1, P = 0.3793 versus control; $brp^{\Delta 190}$, 0.10 ± 0.01, P = 0.2184 versus control and P = 0.5979 versus $brp^{\Delta 170}$; *n* = 20 NMJs in seven larvae/genotype. All quantifications except D are normalized to control. Error bars represent SEMs. n.s., P > 0.05, Mann–Whitney *U* test. *n* is as indicated in the bars.

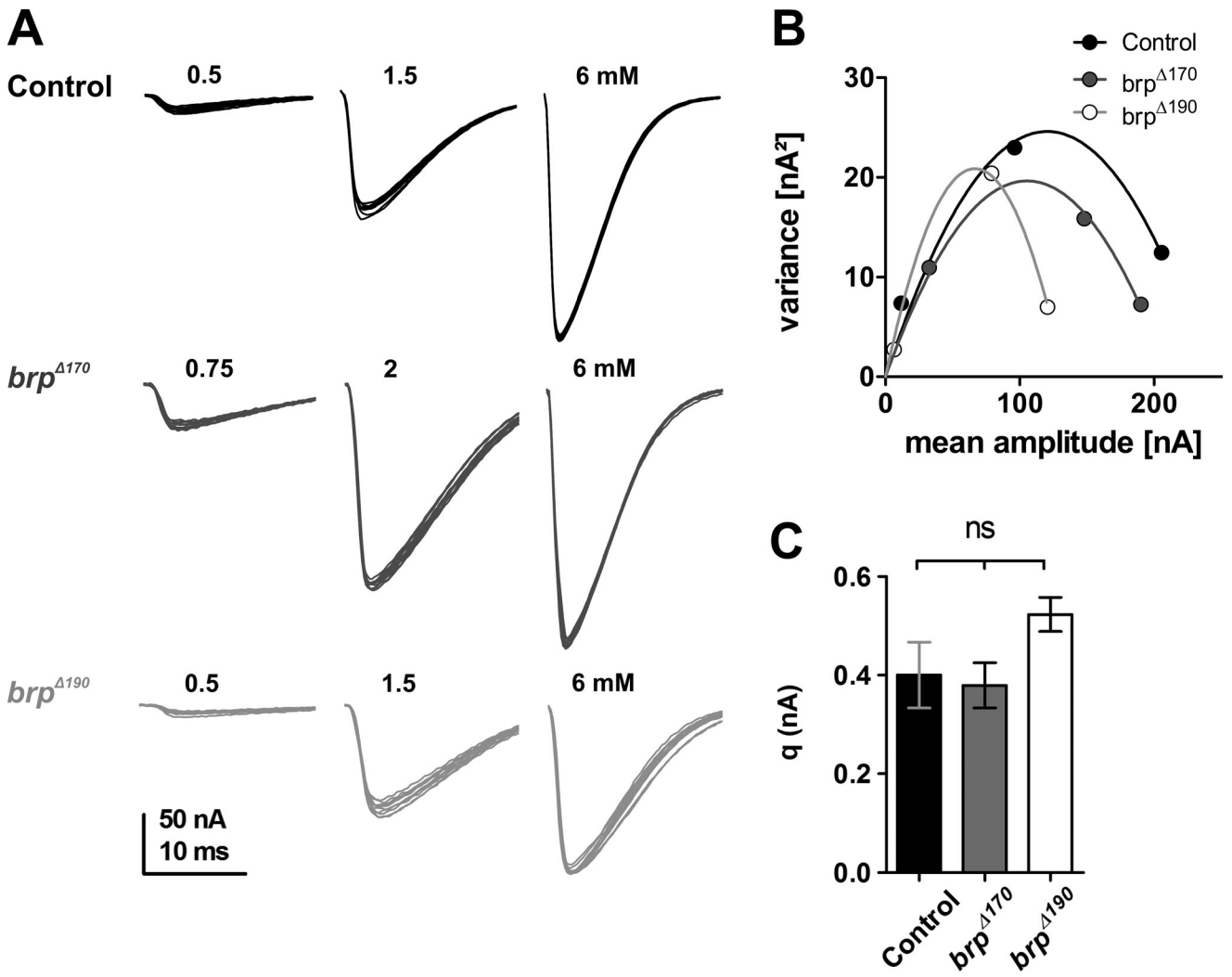

Figure S3. **Variance–mean analysis of BRP isoform mutants.** (A) Example traces for Control, $brp^{\Delta 170}$, and $brp^{\Delta 190}$ ($n \geq 20$ traces each; Ca^{2+} concentrations as indicated). (B) Parabolic fits of variance–mean analysis of example cells in A. (C) Quantifications of quantal size determined by variance–mean analysis (control, 0.40 ± 0.07, $n = 8$; $brp^{\Delta 170}$, 0.38 ± 0.05, $P > 0.05$, $n = 8$; $brp^{\Delta 190}$, 0.52 ± 0.03, $n = 8$, $P > 0.05$; one-way ANOVA Tukey's posttest). The graph shows mean values with errors bars representing SEMs; n.s., $P > 0.05$.

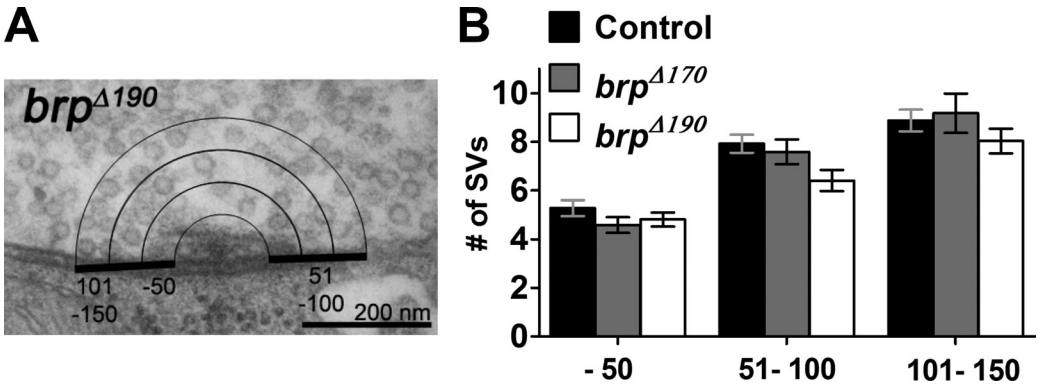

Figure S4. **Cytomatrix distal and lateral SV distribution is not affected in BRP isoform mutants.** (A) The number of SVs within three shells each of 50-nm thickness surrounding the cytomatrix was counted. (B) Quantification of the number of SVs within three 50-nm shells surrounding the cytomatrix. −50 nm: control, 5.3 ± 0.3 (*n* [AZs] = 25); $brp^{\Delta 170}$, 4.6 ± 0.3 (*n* [AZs] = 17); $brp^{\Delta 190}$, 4.8 ± 0.3 (*n* [AZs] = 32); P = 0.3358, Kruskal–Wallis ANOVA. 51–100 nm: control, 7.9 ± 0.4 (*n* [AZs] = 25); $brp^{\Delta 170}$, 7.6 ± 0.5 (*n* [AZs] = 17); $brp^{\Delta 190}$, 6.4 ± 0.4 (*n* [AZs] = 32); P = 0.0727, Kruskal–Wallis ANOVA. 101–150 nm: control, 8.9 ± 0.5 (*n* [AZs] = 25); $brp^{\Delta 170}$, 9.2 ± 0.8 (*n* [AZs] = 17); $brp^{\Delta 190}$, 8.0 ± 0.5 (*n* [AZs] = 32); P = 0.3710, Kruskal–Wallis ANOVA. Error bars represent SEMs. n.s., P > 0.05.

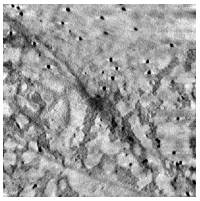

Video 1. **Control T-bar structure.** Electron microscope tomography reconstruction of wild-type larval NMJ terminals. Sections of second instar larvae (250 nm thick) were prepared by HPF/FS. Tilt series were acquired on a microscope (Tecnai Spirit) at a nominal magnification of 30,000 at 3–5-µm defocus using Xplore3D.

Video 2. ***brp*$^{\Delta 170}$ T-bar structure.** Electron microscope tomography reconstruction of $brp^{\Delta 170}$ larval NMJ terminals. Sections of second instar larvae (250 nm thick) were prepared by HPF/FS. Tilt series were acquired on a microscope (Tecnai Spirit) at a nominal magnification of 30,000 at 3–5-µm defocus using Xplore3D.

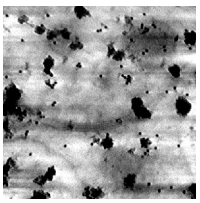

Video 3. ***brp*$^{\Delta 190}$ T-bar structure.** Electron microscope tomography reconstruction of $brp^{\Delta 190}$ larval NMJ terminals of control animals. Sections of second instar larvae (250 nm thick) were prepared by HPF/FS. Tilt series were acquired on a microscope (Tecnai Spirit) at a nominal magnification of 30,000 at 3–5-µm defocus using Xplore3D.